# Putative Global Minimum Structures of Morse Clusters as a Function of the Range of the Potential: $161 \leq N \leq 240$

**Yan Feng,*,†,‡ Longjiu Cheng,*,‡ and Haiyan Liu†**

*Hefei National Laboratory for Physical Sciences at the Microscale, and School of Life Sciences, University of Science and Technology of China (USTC), Hefei, Anhui, 230027, China, and School of Chemistry & Chemical Engineering, Anhui University, Hefei, Anhui, 230039, China*

*Received: May 26, 2009; Revised Manuscript Received: October 19, 2009*

We have located the structures of putative global minima for Morse clusters as a function of the range of the potential and the cluster size (with atom number $161 \leq N \leq 240$) using the dynamic lattice searching method. Our work indicates that with the range of the potential decreased, the structure of global minimum changes from disordered to icosahedral to decahedral to close-packed, and meanwhile the size effect on structures becomes weaker. At the middle range of potential, the icosahedral structures with Mackay overlayers are more predominant than those with anti-Mackay overlayers. The conformational analysis of $M_{200}$ at different $\rho_0$ is given to get the funnel information of the energy landscape. The energy sequences of global minima at different $\rho_0$ are studied to find out the magic numbers, and the zero temperature "phase diagram" is given for an overall view of how the global minima depend upon $N$ and $\rho_0$.

## 1. Introduction

The theoretical or experimental field of cluster science has attracted a lot of interests. The studies on the structures of clusters with increasingly larger sizes can eventually bridge the gap between isolated atoms/molecules and bulk material in a comprehensible manner. In fact, there is no direct experimental method for determining the structures of large free clusters, and in addition, the analysis of experimental data to obtain structural information always relies on comparison with the theoretical prediction of structural models,[1−4] so the theoretical prediction becomes more and more important. Many theoretical investigations on the structures of different clusters were carried out by computational methods. Wales group made a systematic research on the potential energy surface (PES) of various cluster systems, such as water clusters,[5] $C_{60}$ clusters,[6] and metal clusters,[7] and built the Cambridge Cluster Database.[8] The C clusters with Brenna potential,[9] the Au clusters,[10] the magic nanoalloy clusters,[11,12] and the boron nitrides clusters[13] were also modeled.

A lot of work mentioned above detailedly describes the global minima or low-lying motifs on PES to locate the ground state for a physical system. There are also some reports about the effect of the range of the potential on the structures or phase behavior of different systems.[14−19] As the potential range is decreased, the number of minima and saddle points on the PES increases and the PES becomes rugged;[20−23] meanwhile the predominant global minimum structures are also changed. Therefore the range of the potential is a key parameter to determine the structures of various clusters. For example, at small cluster size, the most favored motifs of sodium clusters with a long-ranged interaction are disordered and icosahedral;[24] for Lennard-Jones (LJ) clusters with a middle-ranged interaction, the most favored motifs are icosahedral and only at some magic numbers decahedral, face-centered cubic, and tetrahedral motifs can be global minima;[8] for $C_{60}$ molecular clusters with a very short-ranged interaction, the predominant structures are decahedral, tetrahedral, and close-packed.[25,26]

The structural knowledge of clusters with intermediate size (containing from hundreds to thousands of atoms) is important to achieve a deep understanding of clusters and reveal the structural evolution with the increase of cluster size. However, in all but the simplest cases, this problem is very complicated, because the number of local minima tends to grow exponentially with the increase of cluster size. Also many empirical potentials are too complicated to provide a physical insight into the observed structures. Consequently, the simple model potential is usually used to understand the structures of clusters with large size, such as Morse potential[27] and LJ potential.[28−30]

Morse potential is simple and convenient enough that it is widely used as a test system to investigate the effect of the range of the potential on the structures or phase behavior of the clusters by varying a single parameter.[31−36] Using Morse potential, Doye et al.[37] made a systematic study on how the range of the potential affects the global minimum structures. They located the structures of putative global minimum as a function of the range of the potential and gave out the structural phase diagram for cluster size $N \leq 80$. Later on, the putative global minima of Morse clusters for $N \leq 160$ were found with a more efficient algorithm, and a number of new putative global minima were also given for $N \leq 80$.[38] The optimal strain-free close-packed isomers of Morse clusters at a very short potential range for cluster size $10 \leq N \leq 250$ were also modeled.[39] However, less is known about the global minimum structures above that size as a function of the range of the potential. The studies on the sequences of the global minima as a function of $\rho_0$ and $N$ for larger size of Morse clusters may provide a particularly convenient laboratory for studying general characteristics of multidimensional potential surfaces, so we continue to give the results for larger Morse clusters at $161 \leq N \leq 240$. These structures will be of considerable interest to experimentalists working on gas phase clusters and to groups studying global optimization of clusters.

* Corresponding authors. E-mail: fy@ustc.edu. Tel/Fax: +86-551-5107342. E-mail: clj@ustc.edu. Tel/Fax: +86-551-5107342.
† University of Science and Technology of China.
‡ Anhui University.

10.1021/jp904925j CCC: $40.75 
Published on Web 11/12/2009

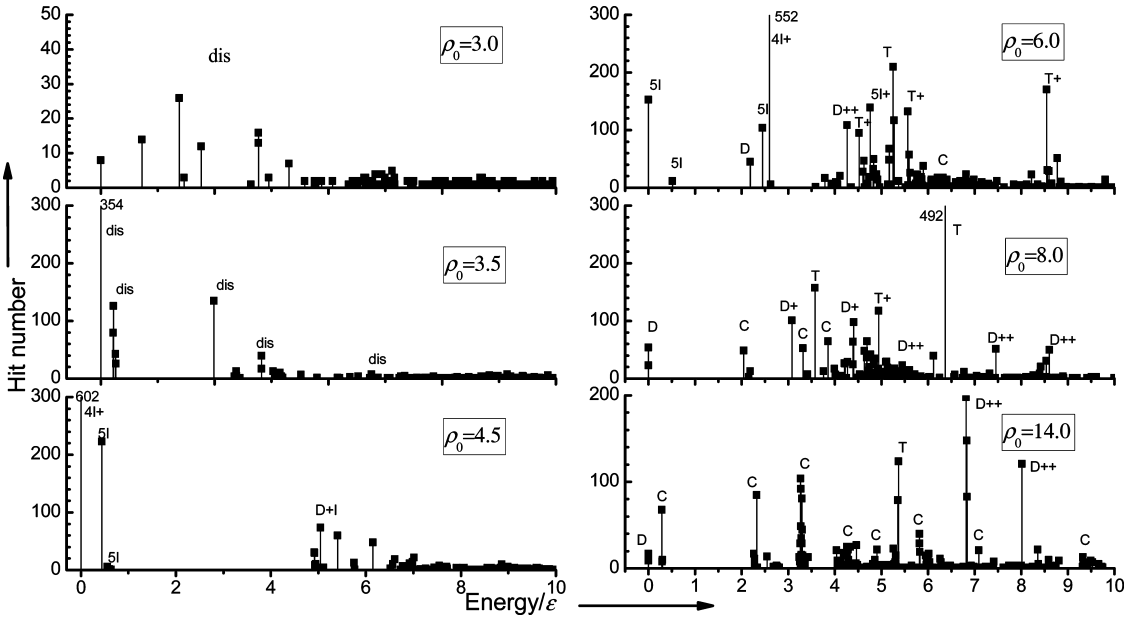


**Figure 1.** Structural distributions of $M_{200}$ clusters in 10 000 DLS runs for $\rho_0 = 3.0$, 3.5, 4.5, 6.0, 8.0, and 14.0 (as labeled). The *y*-axis gives the hit numbers of various metastable local minima. The *x*-axis gives relative energy from the global minimum structure. The hit numbers out of range are labeled in the figure.

## 2. Computational Methods

Morse potential[40] can be taken as a test system with pair interaction, which can be written as

$$E(r) = \varepsilon \cdot e^{\rho_0(1-r/r_e)}[e^{\rho_0(1-r/r_e)} - 2]$$

where $\varepsilon$ is the pair well depth, $r_e$ is the equilibrium distance. In reduced units ($\varepsilon = 1$, $r_e = 1$), $\rho_0$ is a single adjustable parameter which determines the range of the potential and the larger $\rho_0$ means more short-ranged interaction.

The dynamic lattice searching (DLS) method is used to locate the global minima of Morse clusters as a function of the range of the potential. The DLS combines the advantages of the lattice searching method and the stochastic unbiased global optimization method. It has been proven to be an efficient unbiased cluster optimization method for LJ clusters,[41] $C_{60}$ molecular clusters,[26] and Morse clusters.[38] The DLS starts with a randomly generated local minimum, and performs a circulation of construction and the searching of the dynamic lattice (DL) until the better solution approaches the best. The DL is constructed adaptively based on the randomly generated local minimum by searching the possible location sites for an added atom, and the DL searching is implemented by iteratively moving the atom located at the occupied lattice site with the highest energy to the vacant lattice site with the lowest energy. Because the DL can greatly reduce the searching space and the number of the time-consuming local minimization procedures, the DLS method runs at a very high efficiency, especially for the clusters of large size. Moreover, DLS can locate the lowest-energy structures of various motifs (e.g., icosahedral, decahedral, and close-packing) instead of only the global minima.[42]

To have a systematic study on the global minimum structures of Morse clusters as a function of the range of the potential, at each $\rho_0$ among 3.0, 3.5, 4.0, 4.5, 5.0, 6.0, 8.0, 10.0, and 14.0, 5000 DLS runs are carried out separately, and the 20 lowest energy minima located in the DLS runs for each $\rho_0$ are recorded. Finally, the putative global minimum structures for potential range $\rho_0 \geq 3.0$ are found out from the recorded minima.

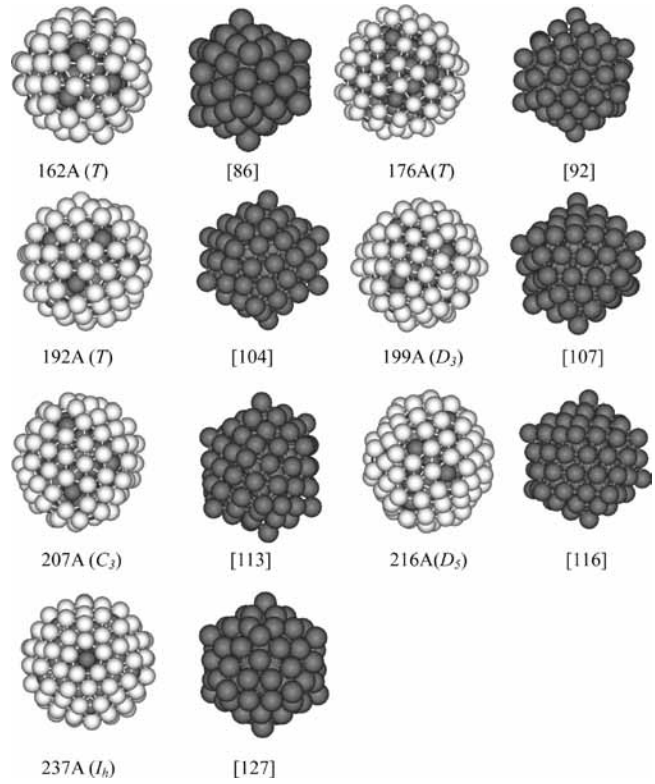


**Figure 2.** Global minima of Morse clusters with disordered packing. The numbers enclosed by "[ ]" are the size of the core.

## 3. Results and Discussion

**3.1. Conformation Analysis of $M_{200}$ as a Function of the Range of the Interaction.** We have carried out the conformational and structural analysis of Morse clusters at atom number $N = 200$ ($M_{200}$) to get the funnel information of the energy landscape and the structural information for various packing styles. Based on the principle of DLS,[42] a conformation with larger hit number lies in a wider funnel on the PES. Figure 1 plots the conformational distribution of $M_{200}$ during 10 000 DLS

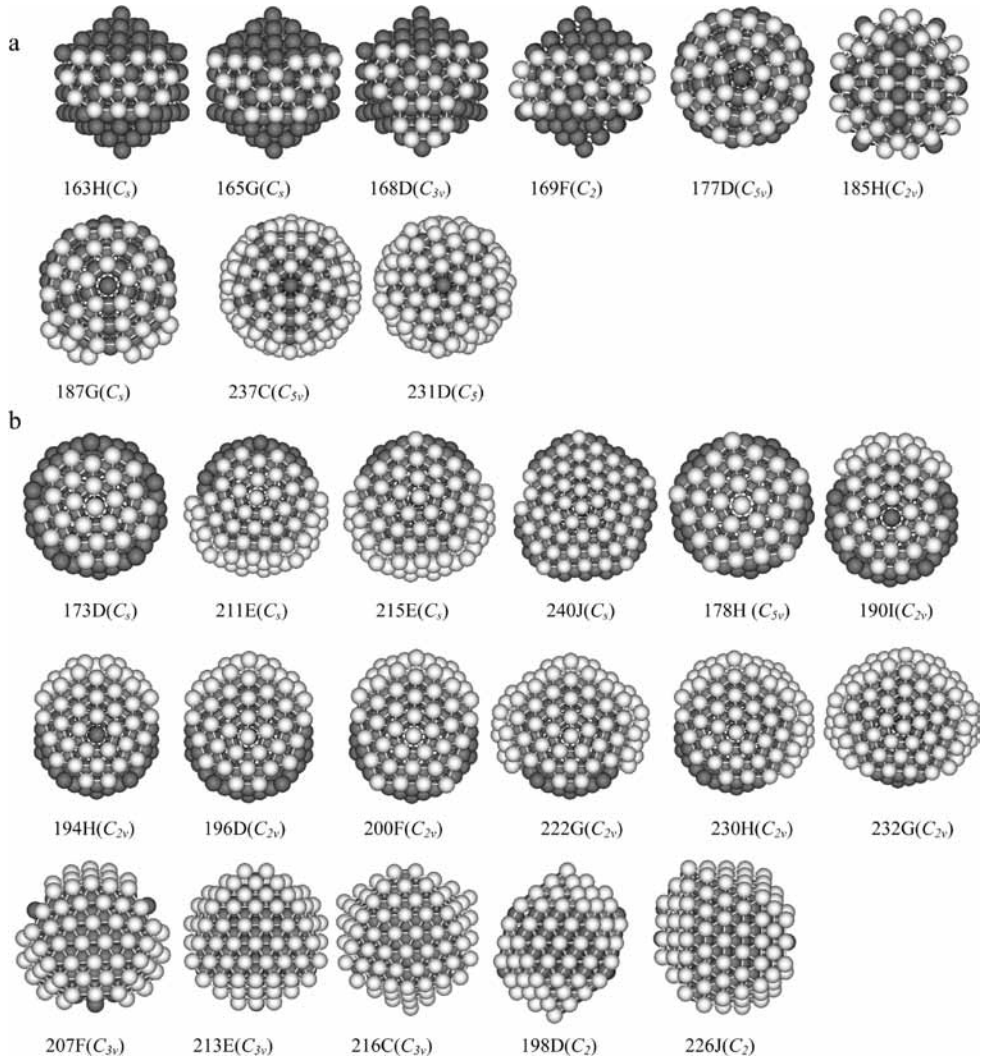


**Figure 3.** Global minima of Morse clusters with icosahedral packing: (a) Ih147 plus anti-Mackay overlayers (4I+); (b) Ih147 plus Mackay overlayers (5I).

runs at $\rho_0 = 3.0$, 3.5, 4.5, 6.0, 8.0, and 14.0 where the 50 lowest energy minima located in the DLS runs for each $\rho_0$ are recorded. The mean CPU time of one successful run at above $\rho_0$ is 12 492.711, 618.448, 306.646, 2297.743, 10 148.308, and 55 402.830 s, respectively. Structures labeled in Figure 1 are classified by the motifs: disordered (dis), Mackay icosahedral (I), I plus anti-Mackay overlayers (I+) where the "+" means the anti-Mackay overlayers, tetrahedral (T), decahedral (D), D plus anti-Mackay overlayers (D+), and close-packed (C). The number ahead of the motifs is the size of basic tetrahedra among the structures.[42]

For $M_{200}$, the located structures are disordered at both $\rho_0 = 3.0$ and 3.5. At $\rho_0 = 4.5$, the icosahedral structures including 4I+ and 5I are predominant on the PES. Both 4I+ and 5I are based on the complete or incomplete magic number 147-atom icosahedron (Ih147). 4I+ is the Ih147 plus antilayers with higher strain energy, but 5I is plus Mackay overlayers with lower strain energy. Also, there are D+I with higher energy and lower hit number, which are the hybrid of icosahedron and decahedron. At the middle range of potential ($\rho_0 = 6.0$), icosahedral packings are still predominant both in hit number and in energy. Meanwhile, with lower hit number and higher energy, several decahedral, tetrahedral, and close-packed structures also begin to appear, which indicates that at the middle range of the potential, the conformations on the PES are quite rich. At $\rho_0 = 8.0$, the global minima are decahedral. There are also some tetrahedral structures with the highest hit number, but energetically in disfavor. At $\rho_0 = 14.0$, D++ has the highest hit number, but the two antilayers on both sides may increase the strain energy, so the global minimum structures are still decahedral.

**3.2. Global Minimum Structures at 161 ≤ *N* ≤ 240.** The global minima of Morse clusters at $161 \leq N \leq 240$ with potential range $\rho_0 > 3.0$ have been located. Their detailed information can also be available from the Supporting Information, where the letters in the alphabetic order after the particle numbers are used to distinguish the different conformations at the same cluster size. Figure 2 plots the structures of magic numbers of the disordered clusters (162A, 176A, 192A, 199A, 207A, 216A, 237A), whose energy is dramatically lower than the average. They all have a core plus a spherical outer shell with high symmetry. 162A, 176A, and 192A have the 86-atom, 92-atom, and 104-atom core with $T$ symmetry, respectively; 199A, 207A, and 216A have the 107-atom, 113-atom, and 116-atom core, respectively; 237A has the 127-atom core with $I_h$ symmetry. This kind of core−shell clusters can be spherical and compact enough, so they are favored for the very long-ranged potential range.

The global minima at the middle range are mainly two kinds of icosahedral structures: 4I+ and 5I shown in Figure 3a,b. 163H, 165G, 168D, 169F, 177D, 185H, 187G, and 237C are

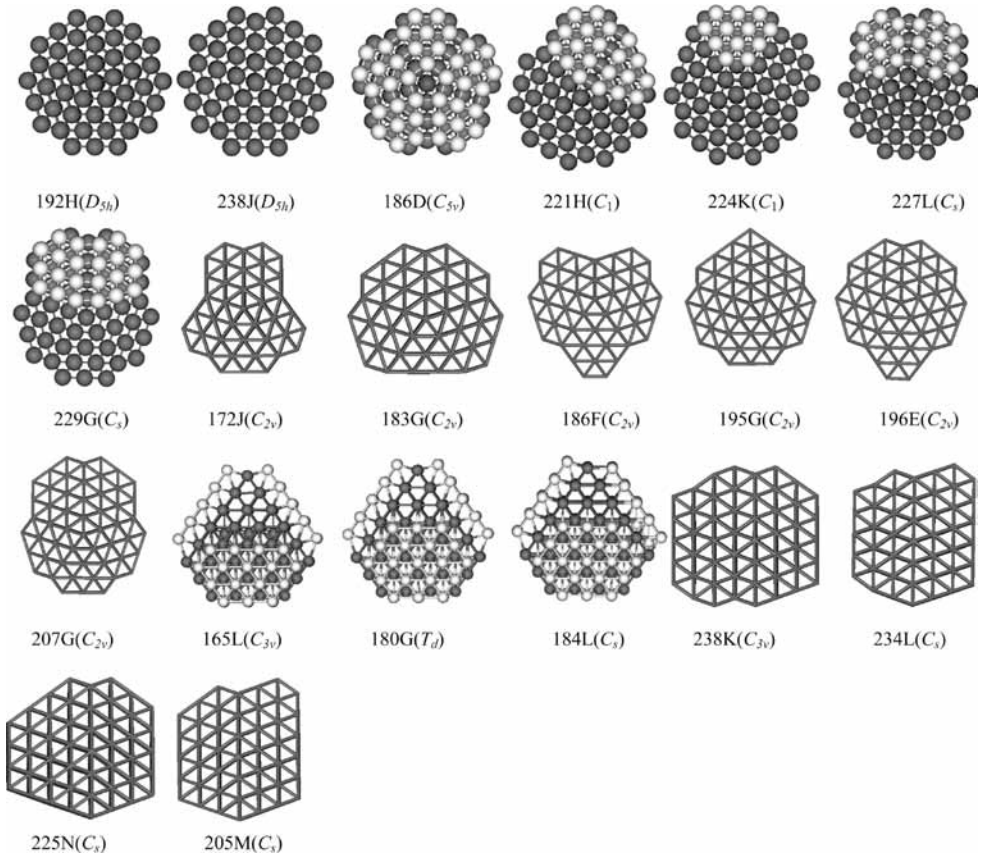


**Figure 4.** Global minima of Morse clusters with Marks decahedral packing, decahedral packing with antilayers, and close-packed packing.

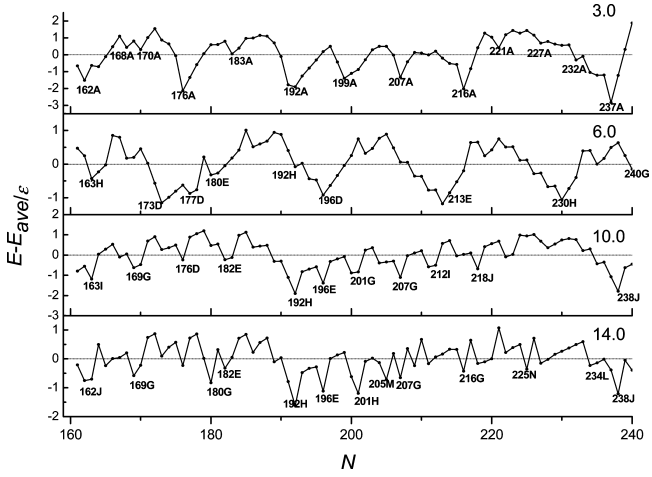


**Figure 5.** Plots of the relative energy of the global minima as a function of cluster size ($161 \leq N \leq 240$) at different $\rho_0$. $E$ is the energy of the global minima, and $E_{ave}$ is a four-parameter fit of the global minima. Downward peaks represent the most stable magic numbers.

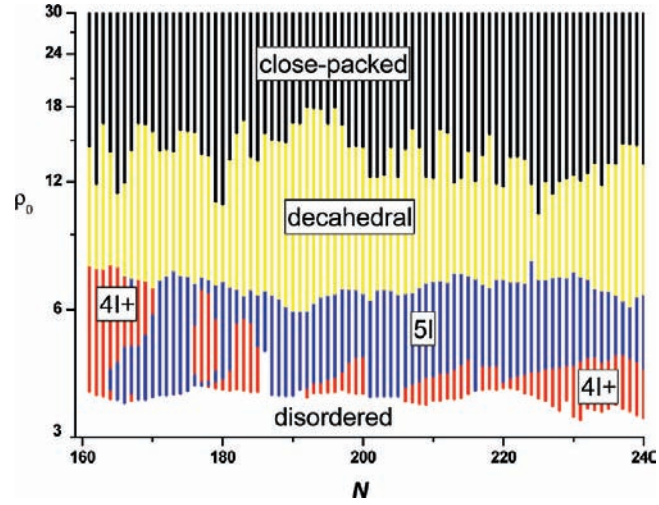


**Figure 6.** Zero temperature "phase diagram" showing the variation of the lowest-energy structures with $N$ and $\rho_0$. Labeled are the structural types: close-packed, decahedral, icosahedral (4I+, 5I), and disordered.

Ih147 plus various regular anti-Mackay overlayers; 231D with $C_5$ symmetry is a distorted 4I+ motif to have more nearest neighbors. 173D, 211E, 215E, and 240J are Ih147 plus Mackay overlayers with $C_s$ symmetry; 178H is with $C_{5v}$ symmetry; 190I, 194H, 196D, 200F, 222G, 230H, and 232G are with $C_{2v}$ symmetry; 207F, 213E and 216C are with $C_{3v}$ symmetry; 198D and 226J are with $C_2$ symmetry. According to the regular structures with the same symmetry (such as 190I, 194H, 196D, and 200F), we can also get some information about where the next atoms will be.

At very large $\rho_0$, the potential is very short-ranged. The icosahedral structure is too strained to be optimal in energy, so the global minima become close-packed or decahedral.[39,43] Most of the lowest-energy close-packed structures at $\rho_0 = 14.0$ located in our work are consistent with the previous results,[39] except 192I, 195I, and 231I. Several decahedral structures and close-packed structures are shown in Figure 4. 192H and 238J are decahedral with $D_{5h}$ symmetry; D+ are decahedral with antilayers on the (111) faces, such as 186D, 221H, 224K, 227 L, and 229G; 172J, 183G, 186F, 195G, 196E, and 207G are decadedral with $C_{2v}$ symmetry; 165 L, 180G, and 184 L are close-packed where the antilayers lie on four (111) faces; 238K, 234 L, 225N, and 205 M are the complete close-packed structures.

**3.3. Sequence Analysis of the Global Minima.** To find out the most stable magic numbers at the different ranges of potential, the energy sequences of the global minima at different $\rho_0$ are plotted in Figure 5. The magic number structures are always with high symmetry. For the very long-ranged potential ($\rho_0 = 3.0$), the most stable structures shown in Figure 2 are disordered. With $\rho_0$ increasing ($\rho_0 = 6.0$), the magic numbers are icosahedral (such as 173D, 196D, 213E, and 230H shown in Figure 3b), and the relative energy of 5I is especially lower than that of 4I+. As the range of the potential is further decreased ($\rho_0 = 10.0$), the strain energy associated with icosahedra increases rapidly and there comes a point where the less strained decahedra become predominant. 192H and 238J with $D_{5h}$ symmetry are the regular Marks decahedral, so their relative energy is especially lower. With $\rho_0$ further increasing ($\rho_0 = 14.0$), most of the magic number structures favor the strain-free close-packed structures.

Figure 6 plots the zero temperature "phase diagram" for $161 \leq N \leq 240$ and $\rho_0 \geq 3.0$ for an overall view of how the global minima depend upon $N$ and $\rho_0$. With $\rho_0$ increasing, the structures of global minima change from disordered to icosahedral, including 4I+ and 5I, to decahedral and to close-packed, and the size effect is less significant. 5I is more predominant than 4I+ at the middle range of potential. The Leary tetrahedron-like structures, which appear in a very narrow range for $N \leq 160$, are not found in this range of cluster size.

## 4. Conclusions

With the dynamic lattice searching method, we have located the putative global minimum structures of Morse clusters for cluster size $161 \leq N \leq 240$ as a function of the range of the potential (with potential range $\rho_0 \geq 3.0$). The energy sequences of the global minima at different $\rho_0$ are studied to find out the magic numbers. The zero temperature "phase diagram" is given for an overall view of how the global minima depend upon $N$ and $\rho_0$. As the range is decreased, the global minimum structures change from disordered to icosahedral, to decahedral, and to close-packed, and the size effect on structures is less significant. The icosahedral structures with Mackay overlayers are more stable than those with anti-Mackay overlayers at the middle range of potential. The global minima of Morse clusters can act as a structural bank, which may be helpful in determining the global minimum structures of other atomic or molecular clusters.

**Acknowledgment.** This work is supported by the National Natural Science Foundation of China (20903001). Y.F. acknowledges the supports from the foundation of Anhui province education department natural research item of China (No. KJ2007B222).

**Supporting Information Available:** Table of the global minima of Morse clusters along with their motifs, energies, point groups, number of nearest-neighbors, strain energies, and the values of $\rho_0$ for which they are probably the lowest energy minimum for $161 \leq N \leq 240$. This material is available free of charge via the Internet at http://pubs.acs.org.

## References and Notes

(1) Calvo, F.; Torchet, G. *J. Cryst. Growth* **2007**, *299*, 374–385.
(2) van de Waal, B. W.; Torchet, G.; de Feraudy, M. F. *Chem. Phys. Lett.* **2000**, *331*, 57–63.
(3) Hewage, J. W.; Amar, F. G.; de Feraudy, M. F.; Torchet, G. *Eur. Phys. J. D* **2003**, *24*, 249–252.
(4) Ikeshoji, T.; Torchet, G.; de Feraudy, M. F.; Koga, K. *Phys. Rev. E* **2001**, *63*, 031103.
(5) Hodges, M. P.; Wales, D. J. *Chem. Phys. Lett.* **2000**, *324*, 279–288.
(6) Doye, J. P. K.; Wales, D. J. *Chem. Phys. Lett.* **1996**, *262*, 167–174.
(7) Doye, J. P. K.; Wales, D. J. *New J. Chem.* **1998**, *22*, 733–744.
(8) Wales, D. J.; Doye, J. P. K.; Dullweber, A.; Hodges, M. P.; Naumkin, F. Y.; Calvo, F.; Hernández-Rojas, J.; Middleton, T. F. http://www-wales.ch.cam.ac.uk/CCD.html.
(9) Cai, W. S.; Shao, N.; Shao, X. G.; Pan, Z. X. *J. Mol. Struct., THEOCHEM* **2004**, *678*, 113–122.
(10) Pyykko, P. *Chem. Soc. Rev.* **2008**, *37*, 1967–1997.
(11) Darby, S.; Mortimer-Jones, T. V.; Johnston, R. L.; Roberts, C. *J. Chem. Phys.* **2002**, *116*, 1536–1550.
(12) Ferrando, R.; Jellinek, J.; Johnston, R. L. *Chem. Rev.* **2008**, *108*, 845–910.
(13) Strout, D. L. *J. Phys. Chem. A* **2000**, *104*, 3364–3366.
(14) Shukla, K.; Rajagopalan, R. *J. Chem. Phys.* **1994**, *101*, 11077–11078.
(15) Mederos, L.; Navascues, G. *J. Chem. Phys.* **1994**, *101*, 9841–9843.
(16) Lomba, E.; Almarza, N. G. *J. Chem. Phys.* **1994**, *100*, 8367–8372.
(17) Hagen, M. H. J.; Frenkel, D. *J. Chem. Phys.* **1994**, *101*, 4093–4097.
(18) Doye, J. P. K.; Wales, D. J. *J. Chem. Soc., Faraday Trans.* **1992**, *88*, 3295–3304.
(19) Wales, D. J. *J. Chem. Soc., Faraday Trans.* **1990**, *86*, 3505–3517.
(20) Braier, P. A.; Berry, R. S.; Wales, D. J. *J. Chem. Phys.* **1990**, *93*, 8745–8756.
(21) Stillinger, F. H.; Stillinger, D. K. *J. Chem. Phys.* **1990**, *93*, 6106–6107.
(22) Stillinger, F. H.; Stillinger, D. K. *J. Chem. Phys.* **1990**, *93*, 6013–6024.
(23) Bytheway, I.; Kepert, D. L. *J. Math. Chem.* **1992**, *9*, 161–180.
(24) Noya, E. G.; Doye, J. P. K.; Wales, D. J.; Aguado, A. *Eur. Phys. J. D* **2007**, *43*, 57–60.
(25) Doye, J. P. K.; Wales, D. J.; Branz, W.; Calvo, F. *Phys. Rev. B* **2001**, *64*, 235409.
(26) Cheng, L. J.; Cai, W. S.; Shao, X. G. *Chem. Phys. Chem.* **2005**, *6*, 261–266.
(27) Wales, D. J.; Doye, J. P. K. *Large Clusters of Atoms and Molecules* **1996**, *313*, 241–279.
(28) Wales, D. J.; Doye, J. P. K. *J. Phys. Chem. A* **1997**, *101*, 5111–5116.
(29) Xiang, Y. H.; Jiang, H. Y.; Cai, W. S.; Shao, X. G. *J. Phys. Chem. A* **2004**, *108*, 3586–3592.
(30) Xiang, Y. H.; Cheng, L. J.; Cai, W. S.; Shao, X. G. *J. Phys. Chem. A* **2004**, *108*, 9516–9520.
(31) Berry, R. S. *J. Phys. Chem.* **1994**, *98*, 6910–6918.
(32) Mainz, D. T.; Berry, R. S. *Mol. Phys.* **1996**, *88*, 709–726.
(33) Rey, C.; Gallego, L. J. *Phys. Rev. E* **1996**, *53*, 2480–2487.
(34) Doye, J. P. K.; Wales, D. J. *J. Chem. Soc., Faraday Trans.* **1997**, *93*, 4233–4243.
(35) Doye, J. P. K.; Wales, D. J. *Science* **1996**, *271*, 484–487.
(36) Doye, J. P. K.; Wales, D. J. *J. Phys. B: At. Mol. Opt. Phys.* **1996**, *29*, 4859–4894.
(37) Doye, J. P. K.; Wales, D. J.; Berry, R. S. *J. Chem. Phys.* **1995**, *103*, 4234–4249.
(38) Cheng, L. J.; Yang, J. L. *J. Phys. Chem. A* **2007**, *111*, 5287–5293.
(39) Cheng, L. J.; Yang, J. L. *J. Phys. Chem. A* **2007**, *111*, 2336–2342.
(40) Morse, P. M. *Phys. Rev.* **1929**, *34*, 57–64.
(41) Shao, X. G.; Cheng, L. J.; Cai, W. S. *J. Comput. Chem.* **2004**, *25*, 1693–1698.
(42) Cheng, L. J.; Cai, W. S.; Shao, X. G. *Chem. Phys. Chem.* **2007**, *8*, 569–577.
(43) Doye, J. P. K.; Wales, D. J. *Chem. Phys. Lett.* **1995**, *247*, 339–347.

JP904925J